Boron concentration prediction from Compton camera image for boron neutron capture therapy based on generative adversarial network

Zhenfeng Hou [a], Changran Geng [a,b,c,*], Xiaobin Tang [a,b,c], Feng Tian [a], Sheng Zhao [a], Jie Qi [a], Diyun Shu [a], Chunhui Gong [d]

[a] *Department of Nuclear Science and Technology, Nanjing University of Aeronautics and Astronautics, Nanjing, 210016, China*
[b] *Joint International Research Laboratory on Advanced Particle Therapy, Nanjing University of Aeronautics and Astronautics, Nanjing, 210016, China*
[c] *Key Laboratory of Nuclear Technology Application and Radiation Protection in Astronautics, Ministry of Industry and Information Technology, Nanjing, 210016, China*
[d] *School of Environmental and Biological Engineering, Nanjing University of Science and Technology, Nanjing, 210094, China*

ARTICLE INFO

ABSTRACT

Prompt gamma monitoring for the prediction of boron concentration is valuable for the dose calculation of boron neutron capture therapy (BNCT). This work proposes to use generative adversarial network (GAN) to predict the boron distribution based on Compton camera (CC) imaging quickly and provide a scientific basis for its application in BNCT. The BNCT and Compton imaging process was simulated, then the image reconstructed from the simulation and the contour of skin from CT are used as input, and the distribution of boron concentration from PET data is set as the output to train the network. The structural similarity, peak signal-to-noise ratio, and root mean square error of the images generated by the trained network are improved significantly, and the ratio of the boron concentration between the tumor area and the normal tissue is improved from 1.55 to 3.85, which is much closer to the true value of 3.52. The trained network can optimize the original image within 0.83 s, which is much faster than iterative optimization. The proposed method could help to ease the current online monitoring problem of boron concentration on a computational level, thereby promoting the clinical development of BNCT technology.

1. Introduction

Boron neutron capture therapy (BNCT) is a binary radiotherapy modality that has unique advantages in the treatment of surface tumors and metastatic tumors (Moss, 2014; Sauerwein et al., 2012). Recently, accelerator-based BNCT (AB-BNCT) has developed rapidly, and research on the therapeutic effect of AB-BNCT has attracted more attention (Nakagawa, 2001). The distribution of boron concentration has a great influence on the dose delivered to the patient during BNCT treatment, which is directly related to the therapeutic effect. Therefore, the boron concentration for BNCT needs to be monitored. Many studies have been conducted on the boron concentration measurement methods, which can be roughly divided into two types: offline and online measurements. The offline measurement methods, such as magnetic resonance imaging and inductively coupled plasma atomic emission spectrometry (ICP-AES) (Wittig et al., 2008; Verbakel et al., 2001; Laakso et al., 2001; Raaijmakers et al., 2009), can only measure the boron concentration distribution before or after treatment, but cannot monitor the online

boron concentration.

Online boron concentration measurement methods have been proposed in recent years. Watabe et al. established a practical method to estimate the absolute boron concentration (Watabe et al., 2017), and Balcerzyk et al. proved the feasibility of using ^{18}F-boronophenylalanine positron emission tomography (PET) to monitor boron concentration through experiments (Balcerzyk et al., 2020). The imaging of 0.478 MeV prompt γ rays emitted through ^{10}B (n, α)^{7}Li reaction was also proposed to be used for boron imaging during BNCT treatment, and the single-photon emission computed tomography (SPECT) system used for BNCT dose monitoring has been explored. Kobayashi et al. proposed to combine the SPECT technique with prompt gamma-ray analysis (PGA) to provide an ideal dose estimation system for BNCT (Kobayashi et al., 2000). The strategy of selecting an optimal detector material for prompt gamma (PG) imaging during BNCT with three conclusions has been studied to improve the accuracy of dose estimation (Murata et al., 2011; Minsky et al., 2009). However, SPECT is limited by the heavy collimator and an unsuitable range of detectable energy (i.e., below 300 keV),

---

which can cause problems such as low detection efficiency and poor imaging quality when detecting 0.478 MeV PG during BNCT (Fujieda et al., 2020). Compared with PET and SPECT, the Compton camera (CC) does not require a physical collimator, and the detectable energy range is from keV to several MeV. As a result, the reconstructed image of PG rays detected by CC can be better than that of SPECT and PET in BNCT theoretically.

CC is a γ-ray detector based on electronic collimation with the advantages of high imaging efficiency, high sensitivity, and wide field of view (Jiang et al., 2015; Muraishi et al., 2020; Nakano et al., 2020; Williams, 2016). Some research proposed the use of CC to monitor the boron distribution during BNCT treatment, and the feasibility has been demonstrated by Monte Carlo simulations. Gong et al. optimized the structural design of CC through Monte Carlo simulation to improve detection efficiency during BNCT (Gong et al., 2017). Taewoong et al. used a multiple-scattering CC to monitor the distribution of PG rays in BNCT. Research shows that image quality is important for dose evaluation (Taewoong et al., 2015). However, traditional simple back-projection (SBP) and iterative reconstruction algorithms have problems with poor image quality or long-time consumption, which is not conducive to the application of BNCT online boron concentration monitoring. Research on various algorithms has been conducted to improve the image reconstruction quality of CCs. Voichita et al. studied the influence of system matrix and sensitivity calculation strategies on the quality of the reconstructed images (Ortega et al., 2015). Sato et al. used super-resolution algorithms to improve the imaging quality of CC, but their research is a simulation of simple point sources (Sato et al., 2020). Basalyga et al. used deep learning to sort the absorption events and scattering events of CC, reducing the proportion of error events (Basalyga et al., 2021). However, the source conditions of these studies are ideal, and whether the algorithms proposed in these studies are suitable for BNCT clinical environment remains to be studied.

The PG imaging method can directly measure the distribution of boron dose produced by the reaction of thermal neutrons with ^{10}B, but the boron dose only accounts for 60%–80% of the total dose. Direct prediction of boron concentration can more effectively assess the total dose distribution received by the patient. Generally, because the distribution of thermal neutron flux in the body is not uniform, it is necessary to calculate the boron concentration distribution based on the distribution of prompt gamma rays, which needs to be divided by the neutron distribution in the body. In fact, for certain BNCT facilities and tumor types, the energy spectrum of the accelerator neutron source and the irradiation method to the patient are almost the same. Due to the low concentration of boron in the tissue, it has almost no effect on the neutron flux and is different. And there is little difference in the distribution of hydrogen in different patients, so the distribution of neutrons in patients under this condition is similar. This research proposes that the neutron flux distribution at different positions can be learned from a large number of training sets through generative adversarial network (GAN), and then the distribution of boron can be predicted based on the input prompt gamma distribution image. In this work, GAN is proposed to improve the reconstructed boron distribution image quality of CC quickly to predict the boron concentration distribution during BNCT treatment. In this study, the PG detection system based on single-layer CdZnTe (CZT) CC prototype is simulated to detect 0.478 MeV PG rays released during BNCT treatment. The reconstructed images and contours of skin from CT data are set as input to the network for training, and the influence of event counts and algorithms on the prediction results is discussed.

2. Materials and methods

2.1. Compton camera configuration

To simulate the CC imaging of the 0.478 MeV photons released in the BNCT process, the model based on the single layer CZT CC prototype

from Kromek D-matrix has been built, the spatial resolution is set to 1.72 mm, and the energy resolution is set to 1.30%. The detector system consists of five detection modules, each module is arranged at 30° intervals and contains four CZT crystals (2 × 2 arrangement), the size of each CZT crystal is $2.2 \times 2.2 \times 1.5$ cm^3, the number of pixels is 11×11, and the pixel pitch is 0.31 mm. In the actual BNCT environment, in addition to the 478 keV signal, many 511 keV gamma rays are also emitted, so the selected detector needs to be able to distinguish photons of two energies. To distinguish between two types of photons, the energy resolution of the detector should be within 6%@511 keV, and the energy resolution of the equipment used in the research can reach 1%@662 keV, which can meet this requirement. In simulations, the detection system is placed 20 cm away from the center of a tumor with a high gamma yield in the phantom, which is head-and-neck tumor model based on patients' PET/CT data. The layout of the model is shown in Fig. 1. In the early stage, this BNCT model was simulated. Under this environment, the share of photons generated by the reaction of neutrons and detector materials accounted for less than 2% of all photons detected, so the influence of neutrons on CC imaging was not considered. In this simulation, the forward direction of the neutron beam is ideal, and some collimation and shielding treatment may be required in actual application.

After the energy deposition information of the photons inside the CC is recorded, the image is reconstructed through the SBP algorithm and the origin ensemble with resolution recovery (OE-RR) iterative algorithm (Yao et al., 2019). Details of the SBP algorithm can be found in the supplement.

2.2. Dataset preparation based on Monte Carlo simulation

In this study, low-count images are optimized through the GAN to achieve the goal of predicting the distribution of boron concentration with high quality. The distribution of boron concentration in the tissue and reconstructed image by the CC with the corresponding contour of skin from CT data is the sample pairs of the training set. The contour of the skin is the boundary information of the patient's cross-section obtained from the CT image. This information is input to the GAN for training to make the GAN more accurately predict the contour of the boron distribution. The actual boron distribution of patients is assumed based on PET/CT images, and the PET/CT datasets of head-and-neck patients are obtained from the Cancer Imaging Archive (TCIA) (https://www.cancerimagingarchive.net/). Due to the limited case data available, this study used data from 22 head and neck cancer cases, 14 cases of head-and-neck cancer (including 4840 images) are used as the training set, 2 cases are used as the validation set, and 6 cases are used as the test set. Generally, a limited number of training sets are prone to overfitting, so data augmentation methods such as horizontal flip, random direction rotation and translation of the data set are implemented to increase the randomness of the training set to enhance the generalization ability of the model. The preparation process of the training set is shown in Fig. 2.

The BNCT process is simulated using Geant4 (version 10.05) Monte Carlo simulation software (Agostinelli et al., 2003). The physicslist used in the simulation is FTFP_BERT_HP with corrections made to G4NeutronHPThermalScattering (Geng et al., 2016). In the simulation, an accelerator neutron source, designed by Neuboron Ltd, is used and the energy spectrum of the neutron source is shown in Fig. 3, which will be used in BNCT clinical treatment trials (Taskaev et al., 2021). The diameter of the neutron source is 12 cm, and the irradiation direction is from top to bottom. The patient tumor model faces downward to receive irradiation. For each patient, we extract the PET data of the patients, take the distribution of the positron drug as the distribution of the boron concentration, and irradiate it with an accelerator neutron source. The PET data are preprocessed by normalizing the concentration of positron drugs from 1 to 100 (i.e., 1–100 ppm) as the distribution of boron concentration. The PET/CT data used in this research is registered. A CT
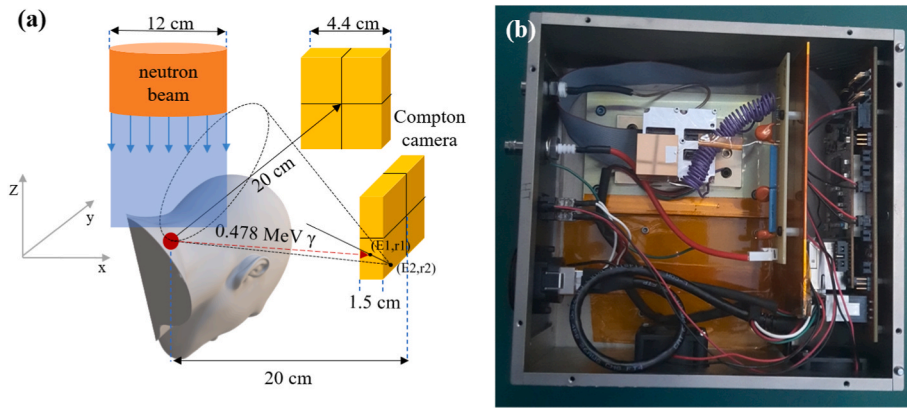
Fig. 1. (a) layout of detecting photons generated in BNCT process with CC. (b) CZT CC prototype.
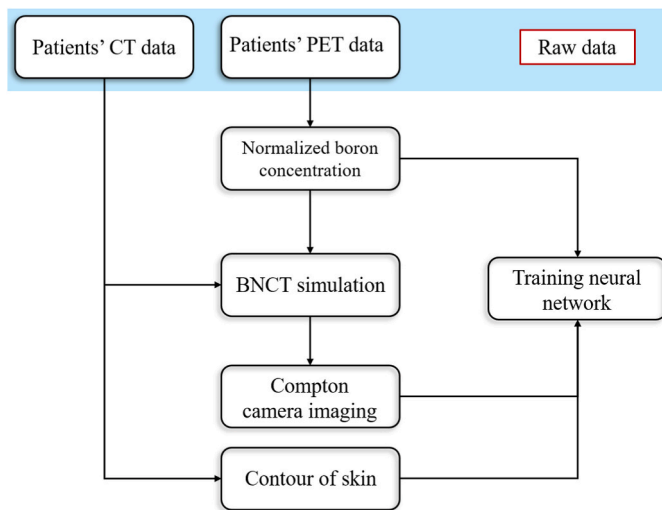

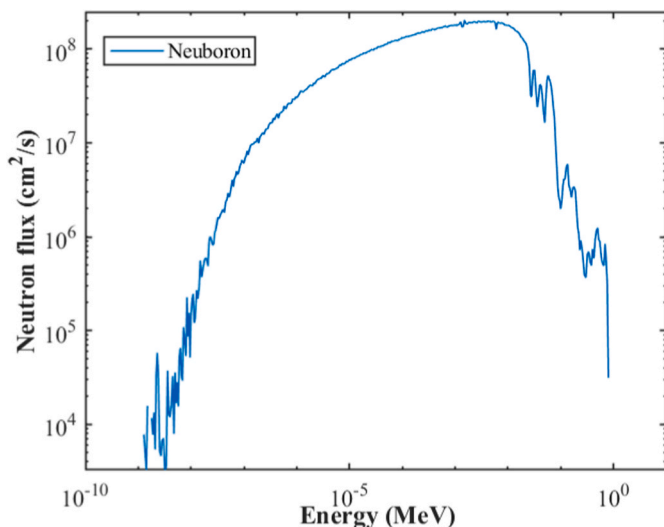**Fig. 2.** Preparation process of the training set.

Fig. 3. Energy spectrum of the neutron source used in simulation.

slice has 512×512 voxels with the voxel size of $0.98 \times 0.98 \times 3.27$ mm, and a PET slice has 128×128 voxels with the voxel size of $3.52 \times 3.52 \times 3.27$ mm. When setting the boron concentration, first match the PET image grid with the CT image grid, then convert the CT value to the

corresponding material number, and convert the PET pixel value to the boron concentration. When Geant4 reads the material file, it reads the CT material and the boron concentration at the same time, then normalizes the material composition. CC is used to detect the 0.478 MeV photons emitted in the BNCT process and reconstruct the PG distribution image. For the BNCT process, there are 8 threads in the simulation, and the number of each thread incident neutrons is 1×10^8, the position and energy of the PG rays are recorded as a phase space file and the resolution of the counting grid is 1 mm. The phase space file is repeatedly used as the source with different random seeds in the detection process.

2.3. GAN structure and evaluation

The GAN model is used in this study, which is trained and evaluated on an NVIDIA TITAN V GPU with 12 GB dedicated RAM, and the Compton image reconstruction is performed on the CPU of intel i7-9750HQ. GAN was first proposed to be used in the field of image conversion and performs well in the prediction of medical images (Goodfellow et al., 2014). The GAN model structure is based on the pix2pix structure of GAN, as shown in Fig. 4.

The generator uses a U-Net network, including four convolutional layers and a maximum pooling layer for downsampling, and then through the up-sampling layer to restore the image to its original size. Compared with ordinary full convolution, U-Net adds skip connection so that the corresponding feature maps and the feature maps after decoding are combined to retain the pixel-level detail information at different resolutions. The objective function of the generator is

$$G^* = \arg \min_G \max_D \ell_{cGAN}(G, D) + \lambda \ell_{L1}(G) \tag{1}$$

where G and D are the loss of generator and discriminator, respectively. The discriminator uses the patchGAN model. The model cuts a picture into multiple patches of the same size, and different patches are independent of each other. The discriminator judges the true and false of each patch, averages the results of all the patches of an image as the final output of the discriminator, and then outputs the final judgment result through the convolutional layer pooling layer. The mean square error between the distribution of the predicted image and the distribution of the target image is used as the loss function of the GAN.

Three indicators structural similarity (SSIM), peak signal-to-noise ratio (PSNR), and root mean square error (RMSE) are used to quantitatively evaluate the resulting images. SSIM is a parameter that reflects visual similarity, and a value close to 1 means that two images are similar to each other.

$$\text{SSIM} = \frac{(2\mu_x\mu_y + K_1)(2\sigma_{xy} + K_2)}{(\mu_x^2\mu_y^2 + K_1)(\sigma_x^2 + \sigma_y^2 + K_2)} \tag{2}$$
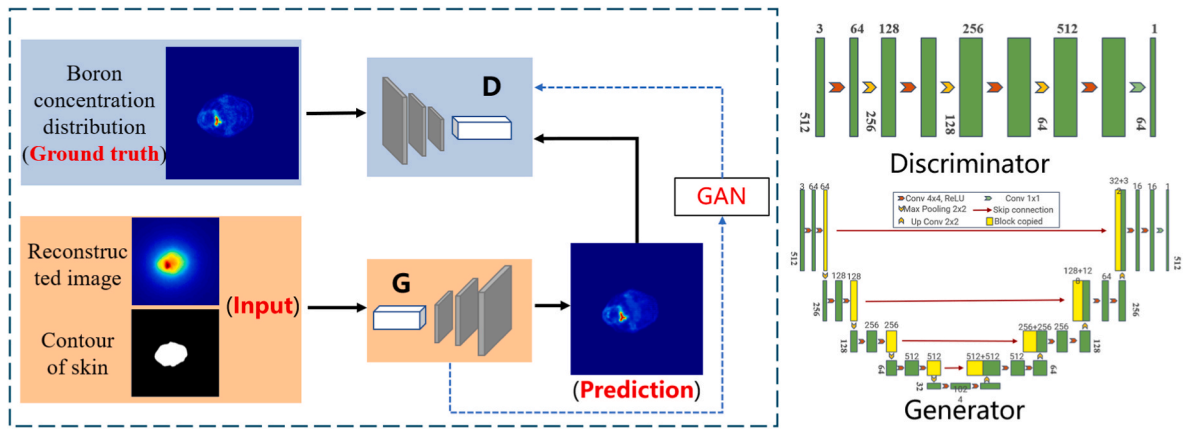
Fig. 4. GAN model structure used in this work.

where μ_x and μ_y represent the average value of image x and y, respectively; σ_x^2 and σ_y^2 represent the standard deviation of x and y, respectively; σ_{xy} is the covariance of x and y; K_1 and K_2 are constants. PSNR represents the image contrast information of the compared images, and a larger PSNR represents smaller distortion. RMSE is the root mean square of the difference in pixel values between the compared images, and a small RMSE indicates a small statistical deviation between the image and the reference image.

$$PSNR = 10\log_{10}\frac{M^2}{MSE} \tag{3}$$

$$MSE = \frac{1}{n}\sum_{i=1}^{n}(V_i^{output} - V_i^{iutput}), RMSE = \sqrt{MSE} \tag{4}$$

where M is the maximum possible pixel value of the picture, and V is the value of the corresponding pixel of the compared images.

3. Results

3.1. Influence of physical condition on the reconstructed image

In the image reconstruction of the CC, the energy of the event and the calculated Compton angle are filtered, which can further improve the image quality. The result of image spatial resolution with filters of different angles and energy when CC is used to image a 0.478 MeV point source is shown in Fig. 5. As shown in Fig. 5, when the energy filter window is too large or too small, the image quality is relatively poor, and
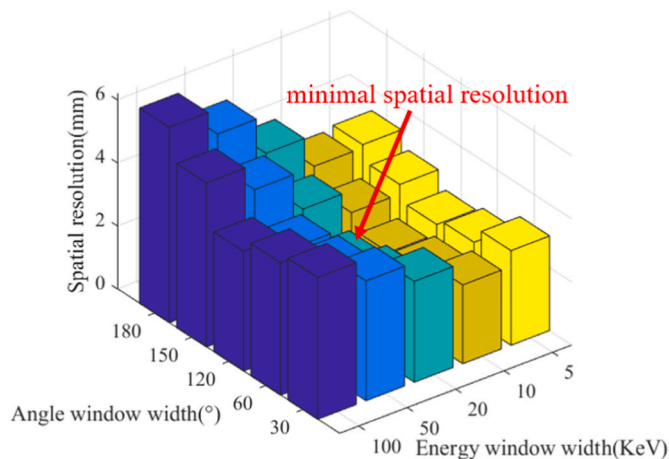

Fig. 5. The spatial resolution of CC with filters of different angles and energy.

the situation is the same as the Compton angle filter window. Therefore, the energy filter window from 0.468 MeV to 0.488 MeV and the Compton angle filter window from 0° to 120° are selected.

In environmental monitoring, a single CC with a smaller size can image a wide range of γ sources, but it will encounter problems in close-range medical applications. In medical applications, the volume of γ source is large, such as a human head and neck case model can be more than 15×15 cm^2. As shown in Fig. 6, compared with 2.2×2.2 cm^2 detector sensitive area, when the sensitive area is 8.8×8.8 cm^2, the distortion phenomenon will be significantly reduced.

3.2. Prediction result of the boron distribution

As a verification of the predict result of the PG distribution, this study compared the predicted result with the actual boron concentration in the simulation. Since the boron concentration distribution data is converted from the PET data, the boron concentration distribution image is similar to the PET image. Fig. 7 shows the input images, the corresponding prediction result, and the real images. The images optimized by GAN are more similar to the real boron distribution images than the images reconstructed with a low number of Compton events. In addition, GAN can quickly optimize the original image in 0.83 s. The average ratio of the boron concentration between the tumor area and normal tissue of the input image is 1.55, and the predicted result is 3.85, which is closer to the true value of 3.52. However, as shown in patient #2 of Fig. 7, GAN will predict the wrong hot spots. This result occurred because the boron concentration of the tumor is low, even close to the normal tissue, then the 0.478 MeV PG rays generated in the tumor area are close to the normal tissue. Thus, the hot spots that represent the tumor area are not prominent enough, which results in inaccurate prediction results. Adding more patient case data of tumors with low boron concentration could potentially improve the results.

3.3. Influence of physical condition on the reconstructed image

Image quality evaluation parameters SSIM, PSNR, and RMSE are used as indicators to evaluate the prediction results of the network. The images reconstructed with SBP from different numbers of events are used as the input of the network, and the indicators of the GAN prediction results are compared. Fig. 8 shows the GAN prediction results of input with different event images. Comparing the initial CC image with 1,000,000 events and GAN optimized image, the SSIM and PSNR are improved from 0.78 to 28.13 to 0.97 and 42.76. On the other hand, after the optimization of the GAN, the SSIM of the prediction results of the GAN is generally above 0.9, and the PSNR is above 40, which shows that the GAN has a significant improvement effect on images. When the number of events is large enough (>100,000), the optimized image with
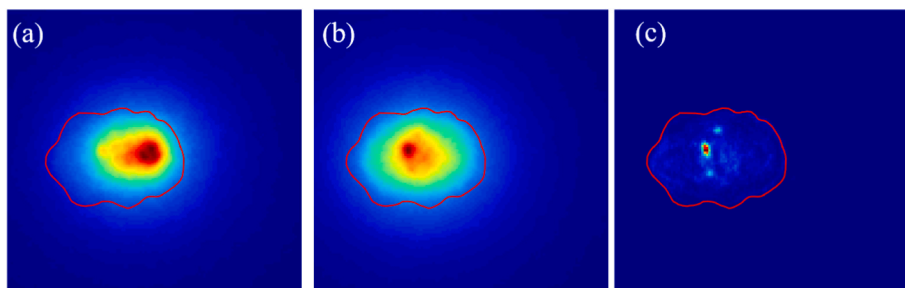
Fig. 6. (a) CC image when the detector size is 2.2 × 2.2 cm². (b) CC image when the detector size is 8.8 × 8.8 cm². (c) The true distribution of the source of 0.478 MeV γ rays.
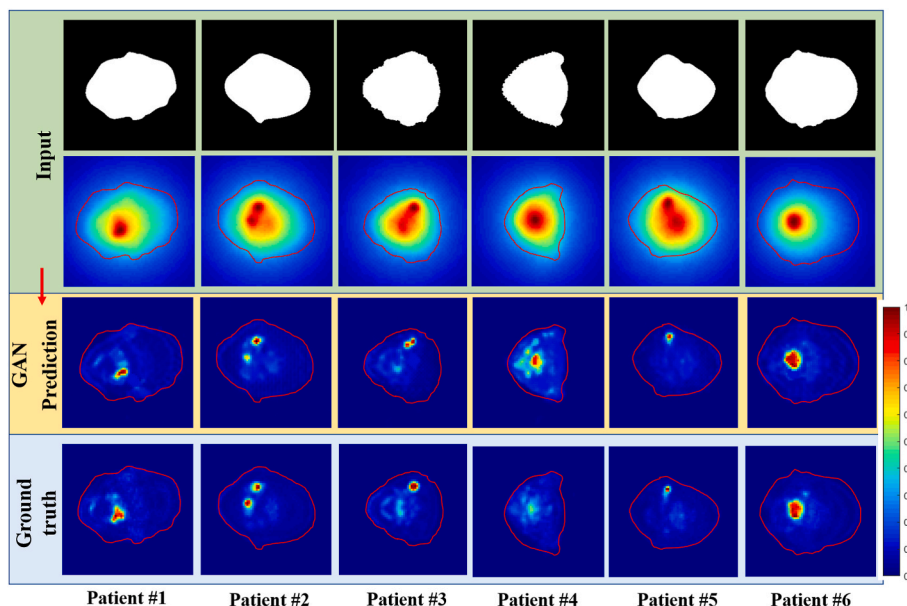

Fig. 7. GAN prediction results of different patients. The CT contours were lined out with a thin red line. (For interpretation of the references to colour in this figure legend, the reader is referred to the Web version of this article.)
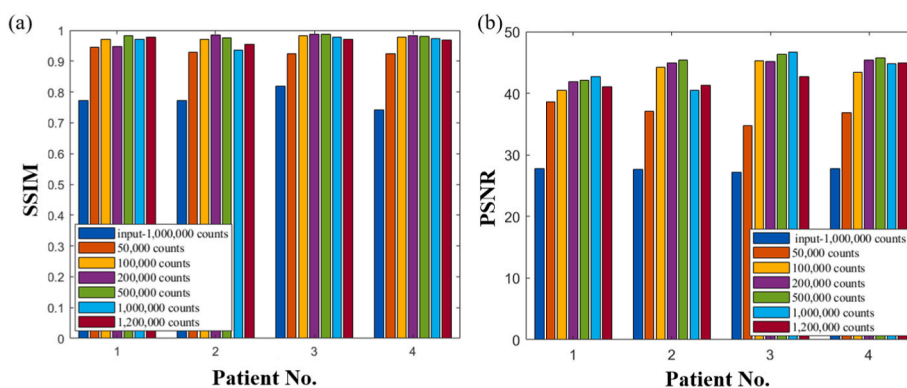

Fig. 8. GAN prediction results of input with different event images: (a) SSIM (b) PSNR.

GAN has no big difference. However, when the reconstructed image of 1,200,000 events is used as input, the quality of the prediction result is reduced overall.

3.4. Prediction results of input images with different algorithm

In addition to SBP, the OE-RR iterative algorithm is also commonly used in CC image reconstruction (Yao et al., 2019). The OE-RR algorithm

is an iterative reconstruction algorithm based on Markov chain, which has good performance in image quality and reconstruction time. A comparison of the prediction results of the OE-RR algorithm of 3 iterations (OE-GAN) with SBP algorithm (SBP-GAN) is shown in Fig. 9, which indicates that OE-GAN is more accurate than SBP-GAN for predicting the boron distribution in the tumor area. When multiple tumors are present, OE-GAN can distinguish them more clearly. However, for the prediction of the ratio of boron concentration between tumor and normal tissue,
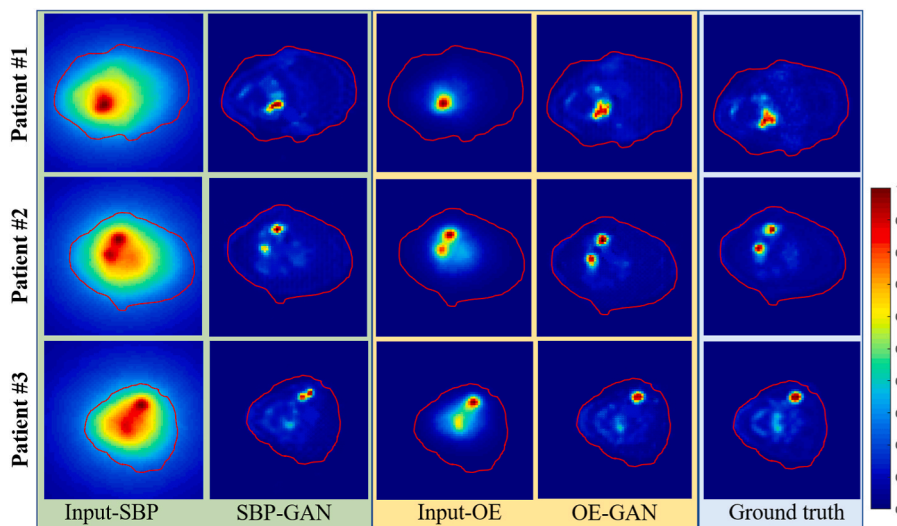
Fig. 9. SBP and iterative algorithm image with GAN prediction results. The CT contours were lined out with a thin red line. (For interpretation of the references to colour in this figure legend, the reader is referred to the Web version of this article.)

OE-GAN usually causes an overestimation due to the underestimation of the boron concentration prediction of normal tissue. As the number of iterations increases, the quality of the prediction results improves. As shown in Fig. 10, The best effect is achieved when iterating three to four times. If the input image has too many iterations, then the boron distribution prediction of normal tissue is worse than the prediction of SBP-GAN and lower than the truth. Moreover, it can be shown in Table 1 that the time consumption of the iterative algorithm is proportional to the number of events; when the number of events is large, the calculation time will far exceed the prediction time of GAN.

4. Discussion

This study proposes to use GAN to predict boron concentration distribution images of CC imaging to provide a scientific basis for using CC to detect online boron concentration distribution in BNCT. Results show that the distribution of the boron concentration predicted by GAN is more similar to true boron distribution in patients than the results reconstructed by SBP or OE-RR algorithms. The results also show the great cost-effective advantage of the proposed method.

The parameters of the CC used in this study are based on the CC prototype of Kromek, and the effect of the sensitive area of the detector on the imaging results is studied. The conclusion is that the sensitive area of detection needs to be adjusted according to the volume and location of the tumor. When the area of a single CC is small, multiple cameras need to be arranged for simultaneous detection. In addition, in

Table 1
Comparison of OE reconstruction with different number of events and GAN.

	OE-10^5 events	OE-5×10^5 events	OE-10^6 events	GAN training	GAN prediction
Time/s	15.36	50.98	182.32	4380	0.83

the iterative algorithm, the sensitivity matrix can be used to correct this error (Williams, 2016), but the sensitivity matrix requires a long time to be obtained through simulation or calculation, which is unrealistic in clinical applications.

The GAN can quickly improve the quality of the reconstructed image, even for images with a small number of Compton events. Compared with SPECT imaging (Fujieda et al., 2020; Yoon et al., 2014), the GAN-based CC images can directly predict the distribution of boron concentration with high quality. The GAN prediction results of SBP images as input with different number of events and OE images as input with different number of iterations are compared. As the number of events increases, the quality of the results predicted by the GAN improves. However, when there are too many events, the quality will decrease, because the distortion of the reconstructed SBP image will be more serious as the number of events increases. Another result is that the prediction of OE-GAN is generally better than SBP-GAN, especially in the tumor area, as shown in Fig. 9. However, when the number of iterations is large, the image will be concentrated in the hot spot area (Maxim et al., 2016), and
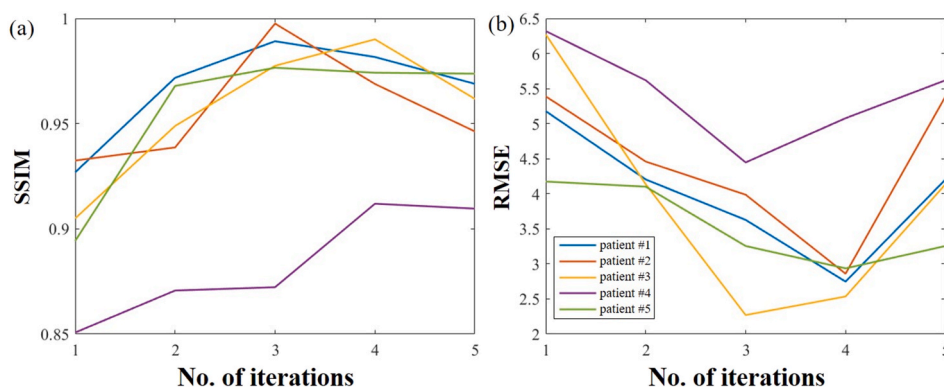

Fig. 10. OE-GAN results of input with different iterations: (a) SSIM (b) RMSE.

the information in the low activity area will be lost due to over-convergence. Therefore, the detection time and the number of OE iterations should be appropriately adjusted according to the boron distribution. Dedicated research efforts should be used to study this topic further.

The SBP algorithm and the OE-RR algorithm are used to reconstruct the initial CC image of 2 interaction events in this study. The algorithm can also be used for image reconstruction of multiple interaction events, and the image can also be used for GAN training. These events affect the reconstruction time of the initial CC images , but are not expected to have an impact on the training and prediction time of the GAN. Therefore, imaging and GAN training using multiple interacting events in future studies may effectively improve the results.

In BNCT, CC does not have high-performance imaging results yet, and using GAN may improve the imaging quality. As the time-consumption of the GAN prediction is within seconds, the online imaging might be able to be realized with this technique. Of course, more solid experiment studies should be performed in the following studies. However, this study still provides some insights for the subsequent clinical translation of the CC in the field of medical imaging. Furthermore, due to the limitation of the development level of PG detection equipment, the Kromek detector may reach saturation under the high flux of neutrons during BNCT, which will seriously affect the detection performance for 0.478 MeV prompt gamma. Winkler et al. proposed that patients could be imaged at low neutron flux (e.g., 1–5% treatment flux) using a PG detection system such as SPECT prior to actual therapeutic irradiation (Winkler et al., 2015). Therefore, the spatiotemporal development of boron distribution in patients can be monitored by CC at low neutron flux to determine the optimal time to initiate therapy in practical applications. Moreover, the detection efficiency of the CC is superior, and it is expected to be used for real-time boron concentration monitoring in the BNCT process in the future.

This study also has limitations. First, the boron concentration distribution assumed in the article is based on the distribution of positron drugs in PET data rather than boroncontaining compounds. The predicted boron concentration is relative boron concentration rather than absolute boron concentration. In future studies, the boron concentration can be more accurately quantified by adding a reference of known boron concentration during the simulation. Second, the head and neck tumors used in this work are located close to the body surface with a simple shape, where the neutron flux near the tumor is high, and the yield of 0.478 MeV gamma rays is much higher than that of normal tissue. Therefore, the network model trained with head and neck tumors may not be suitable for the detection of tumors in other parts such as glioma.

5. Conclusion

This work proposes to use GAN to quickly improve the boron distribution image quality of CC imaging for BNCT boron distribution imaging. The results show that this method can effectively improve the quality of CC images. With the use of this method, the ratio of the boron concentration between the tumor area and the normal tissue is improved from 1.55 to 3.85, which is closer to the true value of 3.52. The image optimized by SSIM can reach 0.95, which is better than 0.80 of SBP. In addition, compared with iterative methods, GAN-based image optimization takes less time, optimizing the original image within 0.83 s. In this work, the feasibility of a GAN-based online monitoring method for BNCT treatment is confirmed. Therefore, the proposed method could help to ease the current online monitoring problem of boron concentration on a computational level, thereby promoting the clinical development of BNCT technology.

CRediT authorship contribution statement

Zhenfeng Hou: Writing – review & editing, Writing – original draft, Validation, Software, Methodology, Investigation, Data curation.

Changran Geng: Writing – review & editing, Supervision, Project administration, Conceptualization. **Xiaobin Tang:** Writing – review & editing, Project administration. **Feng Tian:** Writing – review & editing, Software, Methodology, Data curation, Conceptualization. **Sheng Zhao:** Software, Methodology. **Jie Qi:** Writing – review & editing, Validation. **Diyun Shu:** Writing – review & editing, Software, Methodology. **Chunhui Gong:** Writing – review & editing, Methodology.

Declaration of competing interest

The authors declare that they have no known competing financial interests or personal relationships that could have appeared to influence the work reported in this paper.

Appendix A. Supplementary data

Supplementary data to this article can be found online at https://doi.org/10.1016/j.apradiso.2022.110302.

References

Agostinelli, S., et al., 2003. Geant4—a simulation toolkit. Nucl. Instrum. Methods Phys. Res. Sect. A Accel. Spectrom. Detect. Assoc. Equip. 506, 250–303. https://doi.org/10.1016/S0168-9002(03)01368-8.

Balcerzyk, M., De-Miguel, M., Guerrero, C., Fernandez, B., 2020. Quantification of boron compound concentration for BNCT using positron emission tomography. Cells 9. https://doi.org/10.1002/pamm.202000070.

Basalyga, J.N., Kroiz, G.C., Barajas, C.A., Gobbert, M.K., Maggi, K., Polf, J., 2021. Deep learning for classification of Compton camera data in the reconstruction of proton beams in cancer treatment. Proc Appl Math. https://doi.org/10.1002/pamm.202000070.

Fujieda, K., Kataoka, J., Mochizuki, S., Tagawa, L., Sato, S., Tanaka, R., Matsunaga, K., Kamiya, T., Watabe, T., Kato, H., Shimosegawa, E., Hatazawa, J., 2020. First demonstration of portable Compton camera to visualize 223-Ra concentration for radionuclide therapy. Nucl. Instrum. Methods Phys. Res. Sect. A Accel. Spectrom. Detect. Assoc. Equip. 958. https://doi.org/10.1016/j.nima.2019.162802.

Geng, C., Tang, X., Guan, F., Johns, J., Vasudevan, L., Gong, C., Shu, D., Chen, D., 2016. GEANT4 calculations of neutron dose in radiation protection using a homogeneous phantom and a Chinese hybrid male phantom. Radiat. Protect. Dosim. 168, 433–440. https://doi.org/10.1093/rpd/ncv364.

Gong, C.H., Tang, X.B., Shu, D.Y., Yu, H.Y., Geng, C.R., 2017. Optimization of the Compton camera for measuring prompt gamma rays in boron neutron capture therapy. Appl. Radiat. Isot. 124, 62–67. https://doi.org/10.1016/j.apradiso.2017.03.014.

Goodfellow, I.J., Pouget-Abadie, J., Mirza, M., Xu, B., Warde-Farley, D., Ozair, S., Courville, A., Bengio, Y., 2014. Generative Adversarial Networks, arXiv Preprint arXiv:1406.2661. https://arxiv.org/abs/1406.2661v1.

Jiang, J., Shimazoe, K., Nakamura, Y., Takahashi, H., Shikaze, Y., Nishizawa, Y., Yoshida, M., Sanada, Y., Torii, T., Yoshino, M., Ito, S., Endo, T., Tsutsumi, K., Kato, S., Sato, H., Usuki, Y., Kurosawa, S., Kamada, K., Yoshikawa, A., 2015. A prototype of aerial radiation monitoring system using an unmanned helicopter mounting a GAGG scintillator Compton camera. J. Nucl. Sci. Technol. 53, 1067–1075. https://doi.org/10.1080/00223131.2015.1089796.

Kobayashi, T., Sakurai, Y., Ishikawa, M., 2000. A noninvasive dose estimation system for clinical BNCT based on PG-SPECT–conceptual study and fundamental experiments using HPGe and CdTe semiconductor detectors. Med. Phys. 27, 2124–2132. https://doi.org/10.1118/1.1288243.

Laakso, J., Kulvik, M., Ruokonen, I., Vahatalo, J., Zilliacus, R., Farkkila, M., Kallio, M., 2001. Atomic emission method for total boron in blood during neutron-capture therapy. Clin. Chem. 47, 1796–1803. https://doi.org/10.1093/clinchem/47.10.1796.

Maxim, V., Lojacono, X., Hilaire, E., Krimmer, J., Testa, E., Dauvergne, D., Magnin, I., Prost, R., 2016. Probabilistic models and numerical calculation of system matrix and sensitivity in list-mode MLEM 3D reconstruction of Compton camera images. Phys. Med. Biol. 61, 243–264. https://doi.org/10.1088/0031-9155/61/1/243.

Minsky, D.M., Valda, A.A., Kreiner, A.J., Green, S., Wojnecki, C., Ghani, Z., 2009. Experimental feasibility studies on a SPECT tomograph for BNCT dosimetry. Appl. Radiat. Isot. 67, S179–S182. https://doi.org/10.1016/j.apradiso.2009.03.044.

Moss, R.L., 2014. Critical review, with an optimistic outlook, on boron neutron capture therapy (BNCT). Appl. Radiat. Isot. 88, 2–11. https://doi.org/10.1016/j.apradiso.2013.11.109.

Muraishi, H., Enomoto, R., Katagiri, H., Kagaya, M., Watanabe, T., Narita, N., Kano, D., 2020. Visualization of low-level gamma radiation sources using a low-cost, high-sensitivity, omnidirectional Compton camera. JoVE. https://doi.org/10.3791/60463.

Murata, I., Mukai, T., Nakamura, S., Miyamaru, H., Kato, I., 2011. Development of a thick CdTe detector for BNCT-SPECT. Appl. Radiat. Isot. 69, 1706–1709. https://doi.org/10.1016/j.apradiso.2011.05.014.

Nakagawa, Y., 2001. Frontiers in Neutron Capture Therapy, vols. 73–79. Springer US, ISBN 978-1-4615-1285-1.

Nakano, T., Sakai, M., Torikai, K., Suzuki, Y., Takeda, S., Noda, S.E., Yamaguchi, M., Nagao, Y., Kikuchi, M., Odaka, H., Kamiya, T., Kawachi, N., Watanabe, S., Arakawa, K., Takahashi, T., 2020. Imaging of (99m)Tc-DMSA and (18)F-FDG in humans using a Si/CdTe Compton camera. Phys. Med. Biol. 65, 05LT01 https://doi.org/10.1088/1361-6560/ab33d8.

Ortega, P.G., Torres-Espallardo, I., Cerutti, F., Ferrari, A., Gillam, J.E., Lacasta, C., Llosa, G., Oliver, J.F., Sala, P.R., Solevi, P., Rafecas, M., 2015. Noise evaluation of Compton camera imaging for proton therapy. Phys. Med. Biol. 60, 1845–1863. https://doi.org/10.1088/0031-9155/60/5/1845.

Raaijmakers, C.P.J., Konijinenberg, M.W., Dewit, L., Haritz, D., Huiskamp, R., Philipp, K., Siefert, A., Strcher-Rasmussen, F., Mijnheer, B.J., 2009. Monitoring of blood-10B concentration for boron neutron capture therapy using prompt gamma-ray analysis. Acta Oncol. 34, 517–523. https://doi.org/10.3109/02841869509094017.

Sato, S., Kataoka, J., Kotoku, J., Taki, M., Oyama, A., Tagawa, L., Fujieda, K., Nishi, F., Toyoda, T., 2020. First application of the super-resolution imaging technique using a Compton camera. Nucl. Instrum. Methods Phys. Res. Sect. A Accel. Spectrom. Detect. Assoc. Equip. 969. https://doi.org/10.1016/j.nima.2020.164034.

Sauerwein, W.A., Witting, A., Moss, R., 2012. Neutron Capture Therapy: Principles and Applications. Springer Berlin Heidelberg, ISBN 978-3-642-31333-2, pp. 1–12.

Taewoong, L., Hyounggun, L., Wonho, L., 2015. Monitoring the distribution of prompt gamma rays in boron neutron capture therapy using a multiple-scattering Compton camera: a Monte Carlo simulation study. Nucl. Instrum. Methods Phys. Res. Sect. A Accel. Spectrom. Detect. Assoc. Equip. 798, 135–139. https://doi.org/10.1016/j.nima.2015.07.038.

Taskaev, S., Berendeev, E., Bikchurina, M., Bykov, T., Kasatov, D., Kolesnikov, I., Koshkarev, A., Makarov, A., Ostreinov, G., Porosev, V., Savinov, S., Shchudlo, I., Sokolova, E., Sorokin, I., Sycheva, T., Verkhovod, G., 2021. Neutron source based on vacuum insulated tandem accelerator and lithium target. Biology 10. https://doi.org/10.3390/biology10050350.

Verbakel, W.F.A.R., Rosenschöld, P.M., Ceberg, C.P., Stecher-Rasmussen, F., Persson, B.R.R., 2001. Toward clinical application of PG spectroscopy for in vivomonitoring of boron uptake in boron neutron capture therapy. Med. Phys. 28, 787–795. https://doi.org/10.1118/1.1367281.

Watabe, T., Hanaoka, K., Naka, S., Kanai, Y., Ikeda, H., Aoki, M., Shimosegawa, E., Kirihata, M., Hatazawa, J., 2017. Practical calculation method to estimate the absolute boron concentration in tissues using (18)F-FBPA PET. Ann. Nucl. Med. 31, 481–485. https://doi.org/10.1007/s12149-017-1172-5.

Williams, Z.H.B., 2016. Sensitivity image compensation in pixelated, 3-D position-sensitive CdZnTe detectors. In: 2016 IEEE Nuclear Science Symposium, Medical Imaging Conference and Room-Temperature Semiconductor Detector Workshop (NSS/MIC/RTSD). https://doi.org/10.1109/NSSMIC.2016.8069701.

Winkler, A., Koivunoro, H., Reijonen, V., Auterinen, I., Savolainen, S., 2015. Prompt gamma and neutron detection in BNCT utilizing a CdTe detector. Appl. Radiat. Isot. 106, 139–144. https://doi.org/10.1016/j.apradiso.2015.07.040.

Wittig, A., Michel, J., Moss, R.L., Stecher-Rasmussen, F., Arlinghaus, H.F., Bendel, P., Mauri, P.L., Altieri, S., Hilger, R., Salvadori, P.A., Menichetti, L., Zamenhof, R., Sauerwein, W.A., 2008. Boron analysis and boron imaging in biological materials for Boron Neutron Capture Therapy (BNCT). Crit. Rev. Oncol. Hematol. 68, 66–90. https://doi.org/10.1016/j.critrevonc.2008.03.004.

Yao, Z., Xiao, Y., Chen, Z., Wang, B., Hou, Q., 2019. Compton-based prompt gamma imaging using ordered origin ensemble algorithm with resolution recovery in proton therapy. Sci. Rep. 9, 1133. https://doi.org/10.1038/s41598-018-37623-2.

Yoon, D.K., Jung, J.Y., Jo, H.K., Suk, S.T., 2014. Tomographic image of prompt gamma ray from boron neutron capture therapy: a Monte Carlo simulation study. Appl. Phys. Lett. 104 https://doi.org/10.1063/1.4867338.